

DEFORMATIONS OF THICK TWO-MATERIAL CYLINDER
UNDER AXIALLY VARYING RADIAL PRESSURE

Yakub A. Patel
Sargent & Lundy

SUMMARY

Stresses and deformations in thick, short, composite cylinder subjected to axially varying radial pressure are studied. Effect of slippage at the interface is examined. In the NASTRAN finite element model, multipoint constraint feature is utilized. Results are compared with theoretical analysis and SAP-IV computer code. Results from NASTRAN computer code are in good agreement with the analytical solutions. Results suggest a considerable influence of interfacial slippage on the axial bending stresses in the cylinder.

INTRODUCTION

The analysis of composite (multilayered) cylinders and other axisymmetric bodies with shrink (or press) fit forms an extremely useful class of problem in the design of pressure vessels and various machine components. For example, Figure 1 illustrates a special slipping pipe anchor (Ref. 1) consisting of the clamped (or press fit) support. Figure 2 illustrates a typical bar drawing die composed of an outer hardened steel cylinder press fitted on the inner carbide insert. The loading, in both cases, on the inside surface of the cylinder is variable axial pressure dependent on the seismic motions (Fig. 1) and percentage reductions (Fig. 2) respectively. This paper attempts to present the problem in a generalized way and indicates, in quantitative terms, the effect of interfacial slippage on the various stress components.

SYMBOLS

- E Young's modulus of elasticity, MPa
- ν Poisson's ratio (Note: Suffix 1 refers to inner cylinder and 2 refers to outer cylinder)
- u_r Radial displacements, cm.
- u_z Axial displacements, cm.
- L Length of the cylinder, cm.

Z Axial coordinate
 y,r Radial coordinate
 P Internal pressure, MPa
 k Scale factor for pressure
 σ_{zz} Axial bending stress, MPa
 $\sigma_{\theta\theta}$ Hoop stress, MPa
 σ_{rr} Radial stress, MPa
 a Inside radius, cm.
 b Interface radius, cm.
 c Outside radius, cm.

$$A_1 = (a^2 b^2) / (b^2 - a^2)$$

$$A_2 = b^2 c^2 / (c^2 - b^2)$$

$$B_1 = (b^2 + a^2) / (b^2 - a^2)$$

$$B_2 = c^2 + b^2 / (c^2 - b^2)$$

$$C_1 = A_1 / 2 (1 - \nu_1)$$

$$N_1 = B_1 / (1 + \nu_1) 16$$

$$M_1 = (a^2 + b^2) N_1 + \frac{A_1 C_1}{a^2} \ln \frac{b}{a}$$

M_c = Residual moment for inner cylinder

$$\alpha_1 = \frac{1 + \nu_1}{E_1} \left[-\frac{1}{2} \left(\frac{1 - \nu_1}{1 + \nu_1} \right) B_1 b - \frac{A_1}{b} \right]$$

$$\alpha_2 = \frac{1 + \nu_1}{E_1} \left[-\frac{1}{2} \left(\frac{1 - \nu_1}{1 + \nu_1} \right) b \right]$$

$$\alpha_5 = \frac{1 + \nu_2}{E_2} \left[-\frac{1}{2} \left(\frac{1 - \nu_2}{1 + \nu_2} \right) B_2 b - \frac{A_2}{b} \right]$$

$$\alpha_6 = \frac{1 + \nu_2}{E_2} \left[-\frac{1}{2} \left(\frac{1 - \nu_2}{1 + \nu_2} \right) b \right]$$

ANALYTICAL MODELS

Figure 3 shows the NASTRAN (Ref. 2) finite element model of the composite cylinder. The inner cylinder is of carbide and the outer cylinder is of steel. The model consists of 210 nodes and 168 axisymmetric trapezoidal ring (CTRAPRG) elements. Dimensions and material properties are typical of a bar drawing die used in actual steel drawing process.

The loading consists of an axially varying radial pressure defined by the equation $P = k(Lz - z^2)$. This pressure was input as discrete load on the inside surface using the 'FORCE' card of NASTRAN.

Nodes 91 through 120 are nodes along the interface of the carbide and steel. This interface needs special consideration in the finite element model. In practice, the case is shrinkfitted on the carbide insert, and a large amount of compressive preloading is generated in the relatively brittle carbide insert. This compressive preloading reduces the probability of cracking of the insert during operation.

Since there is no welding (or permanent connection) along the interface, during nonuniform loading, slippage will occur along the mating surfaces. At the interface, compatibility of the radial displacement provides:

$$u_r \Big|_{\text{carbide}} = u_r \Big|_{\text{steel}} \quad \text{for } 0 \leq z \leq L$$

The axial displacement could vary depending on the amount of slippage. Thus

$$u_z \Big|_{\text{carbide}} \neq u_z \Big|_{\text{steel}}$$

NASTRAN (Ref. 3) has a very useful option available through the MPC command. It defines the multipoint constraint of the form:

$$\sum_j A_j u_j = 0 \quad \text{where } A_j \text{'s are the real coefficients and } u_j \text{ are the nodal displacements.}$$

Using this option, the present analysis was carried out on NASTRAN level 15.5 through the UCC 1108 System.

Figure 4 shows the finite element model for the SAP-IV computer code (Ref. 4). This model is similar to the NASTRAN model - however, no slippage can be allowed along the interface. Due to this, the compatibility of deformation along the interface does not represent the actual deformation mode.

THEORETICAL ANALYSIS

A theoretical analysis of this problem is carried out by the author*. In this analysis, the governing equations of three dimension elasticity are

*Being published as a separate paper.

satisfied on the curved surfaces using the series approach of Lee (Ref. 3). The residual elasticity problem is then solved to partially satisfy the boundary conditions on the ends of the cylinder. The compatibility of displacements along the interface is included in such a manner that axial slip is allowed during deformation. The resultant stress components derived are as follows:

$$\begin{aligned} \sigma_{zz} \text{ carbide} &= (-2k_1 + 2k) \left[4N_1 r^2 + (C_1 - 2M_1) + 2C_1 \ln \frac{r}{a} \right] \\ &\quad - \frac{(2k_1 - 2k)}{8(1 + \nu_1)} \left[2r^2 - (a^2 + b^2) \right] + \frac{12}{(b - a)^3} \left(\frac{a + b}{2} - r \right) M_c \\ \sigma_{\theta\theta} &= (k_1 - k)(Lz - z^2) \left[-\frac{B_1}{2} - \frac{A_1}{r^2} \right] - \frac{1}{2} \left[(k_1 + k)(Lz - z^2) \right] \\ &\quad + \nu_1 \left\{ (-2k_1 + 2k) \left[3N_1 r^2 + (C_1 - M_1)(M_1 - a^2 N_1) \frac{a^2}{r^2} + C_1 \ln \frac{r}{a} \right] \right. \\ &\quad \left. - \frac{2k_1 + 2k}{16(1 + \nu_1)} \left[3r^2 - (a^2 + b^2) - \frac{a^2 b^2}{r^2} \right] \right\} + \frac{u_c}{r} E_1 + \nu_1 \sigma_{zz}^R \\ \sigma_{rr} &= \left[(k_1 - k)(Lz - z^2) \right] \left[-\frac{B_1}{2} + \frac{A_1}{r^2} \right] - \frac{1}{2} \left[(k_1 + k)(Lz - z^2) \right] \\ &\quad + \nu_1 \left\{ (-2k_1 + 2k) \left[N_1 r^2 - M_1 + (M_1 - a^2 N_1) \frac{a^2}{r^2} \right. \right. \\ &\quad \left. \left. + C_1 \ln \frac{r}{a} \right] - \frac{2k_1 + 2k}{16(1 + \nu_1)} \left[r^2 - (a^2 + b^2) + \frac{a^2 b^2}{r^2} \right] \right\} \end{aligned}$$

where: $k_1 = \frac{k(\alpha_1 - \alpha_2)}{\alpha_1 + \alpha_2 + \alpha_5 - \alpha_6}$

RESULTS AND DISCUSSIONS

Fig. 5 shows the variation of axial stresses (σ_{zz}) at $r = a, b$ along the length of the inner cylinder. The axial stresses reach their maximum value at the center of the cylinder and the variation is symmetrical about $Z = L/2$ due to the symmetry of the loading. The results from the NASTRAN model are in good agreement with the analytical solution. Further, it may be noted that the results are in better agreement on the inside surface than the outside surface of inner cylinder - the maximum deviations are 2.8% and 8% respectively. This is due to the fact that the inner surface is farther away from the slipping interface thereby less sensitive to the boundary effects.

Variations of the hoop stresses (Figure 6), radial stresses (Fig. 7) and deflections (Fig. 8-9) also indicate good agreement between the analysis and NASTRAN model. At the interface, in Fig. 7, the radial stresses on the outside surface of carbide and inner surface of steel are identical from the analytical solution. In Figure 9, the length is twice the value given in Fig. 3 while the remaining dimensions are the same as Fig. 3.

The effect of slippage at the interface, in quantitative terms, is demonstrated by the values of stresses from SAP IV, NASTRAN and the analytical solution (Table 1). As is indicated by this table, the effect is more pronounced in the values of σ_{zz} - since the slippage makes the bending process more symmetrical.

CONCLUDING REMARKS

The stresses and deformations in composite cylinder subjected to axially varying radial pressure are examined using the NASTRAN finite element models. The MPC feature of NASTRAN is very useful in simulating accurately the slipping interface between carbide and steel. Results from the NASTRAN finite element models and the analytical solutions are found to be in good agreement.

TABLE 1

Stresses in Carbide (Inner) Cylinder (Units: MPa)

Description	Analytical Solution	NASTRAN F.E. Model	SAP IV F.E. Model
<u>At radius = 5.08 cm.</u>			
σ_{zz}	-124.6	-121.0	-136.2
$\sigma_{\theta\theta}$	362.3	366.2	355.0
σ_{rr}	-223.4	-221.8	-220.6
<u>At radius = 6.99 cm.</u>			
σ_{zz}	110.93	102.0	26.2 (Regular) 87.5 (Modified*)
$\sigma_{\theta\theta}$	279.7	275.2	279.2
σ_{rr}	-69.9	-74.4	-72.4

(*Modified using, in steel at interface, one layer of a material having low modulus of elasticity in z direction)

REFERENCES

1. Patel, Y. A.; Cho, F. L.; Dimopoulos, A. P.: Slipping Pipe Anchor - A Novel Design for Piping in High Seismic Intensity Zones - ASME Paper 75-PVP-58, ASME Conf. on Pressure Vessels and Piping, June 1975.
2. C. W. McCormick (Edit.) - The NASTRAN User's Manual - NASA SP-222(01) - National Aeronautics and Space Administration, June 1972.
3. Lee, C. W.: A Theory of Thick Walled Cylinder Under Axisymmetric Loading - Proceedings of the Fourth U. S. National Congress of Applied Mechanics, (ASME) N.Y., 1962, p. 662.
4. Bath, K. J.; Wilson, E. L. and Peterson, F. E.: SAP-IV - A Structural Analysis Program for Static and Dynamic Response of Linear Systems. EERC Report 73-11, University of Calif., Berkeley, June 1973.

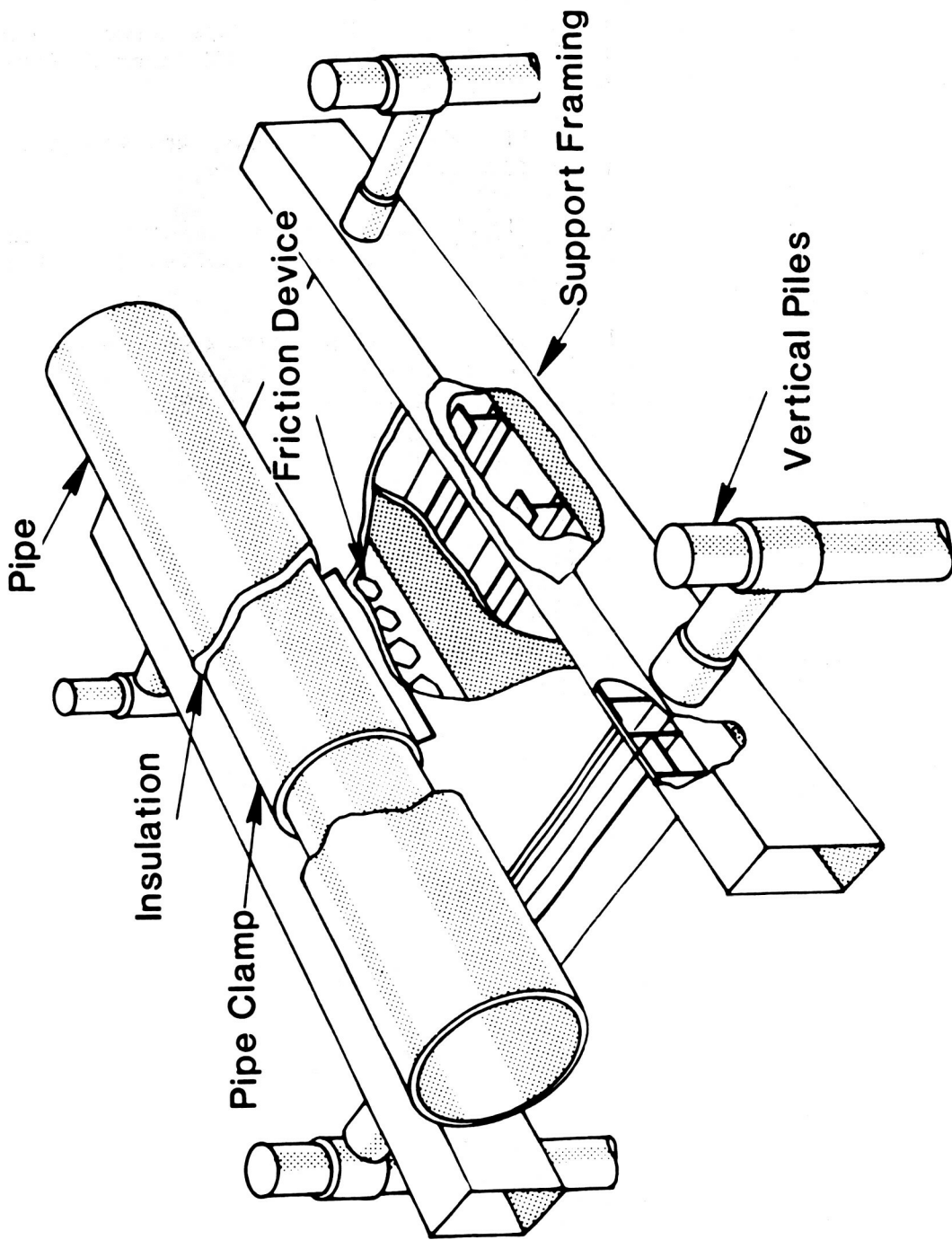


Fig. 1 Slipping pipe anchor.

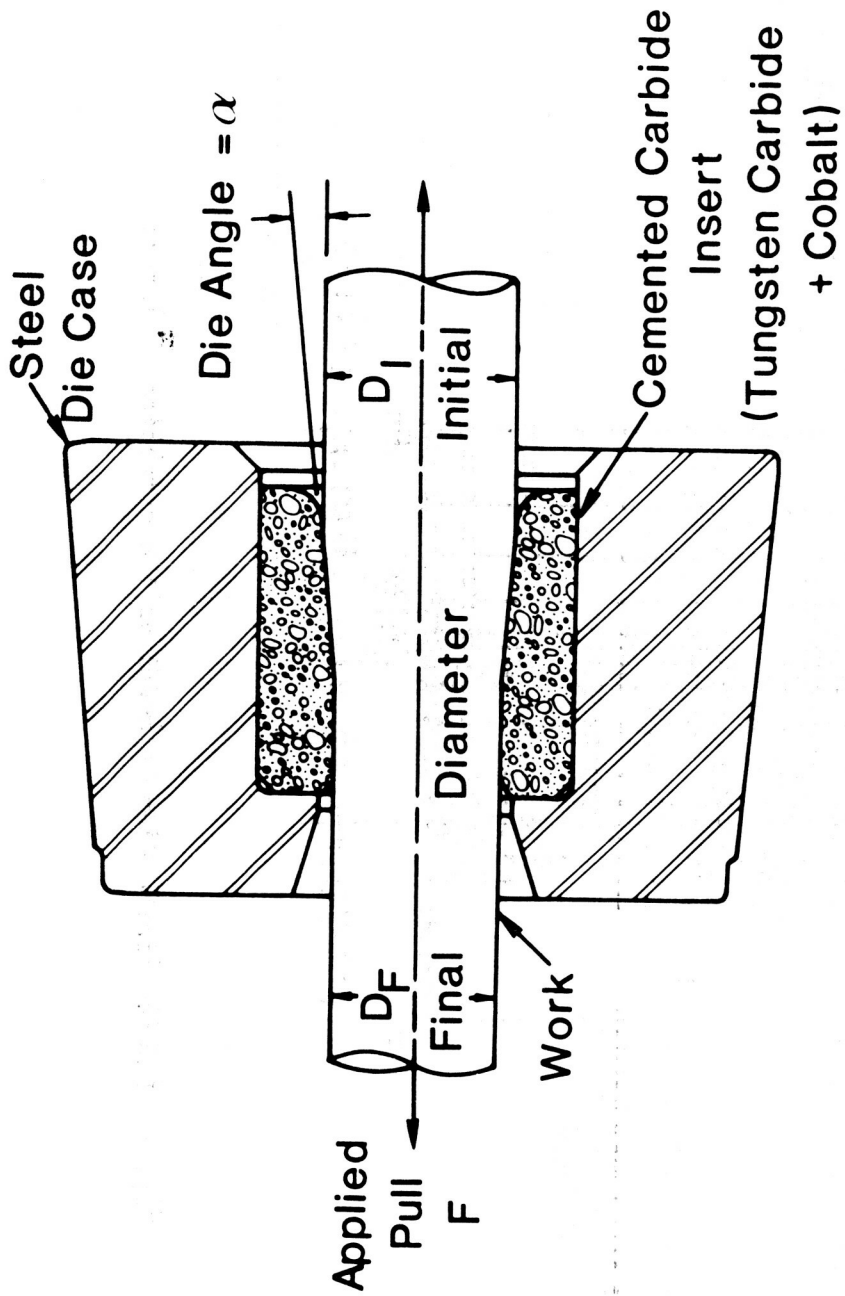


Fig. 2 Section of a typical draw die and workpiece.

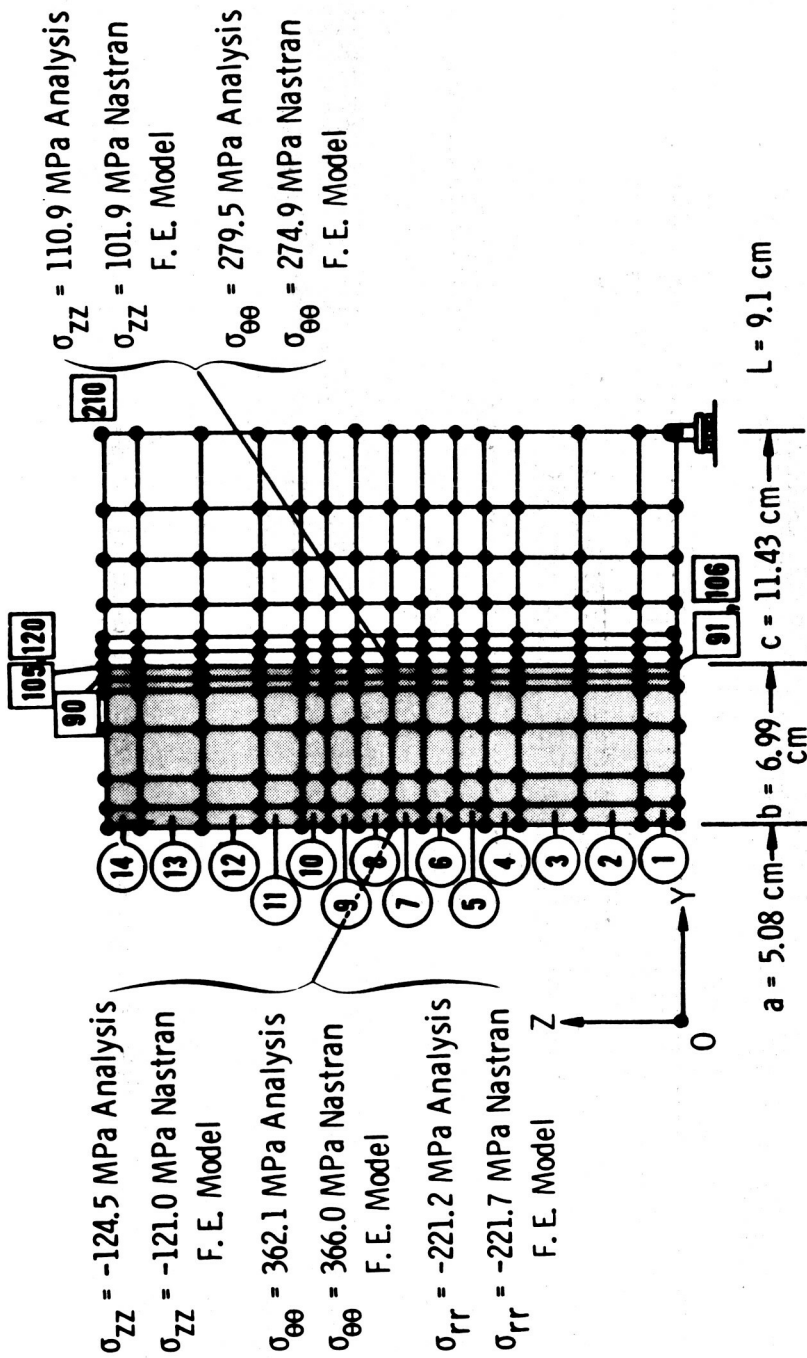


Fig. 3 Nastran finite element model of the composite cylinder.

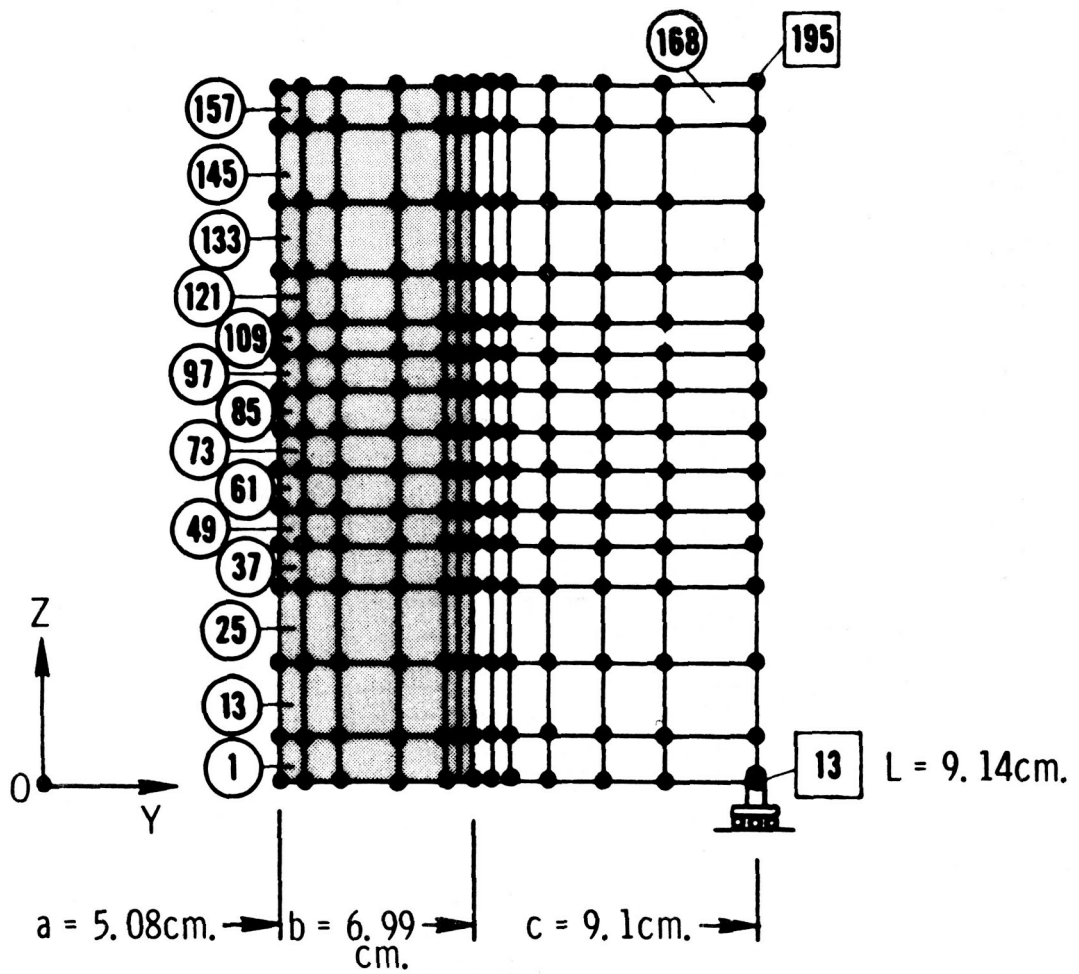


Fig. 4 SAP IV finite element model of the composite cylinder.

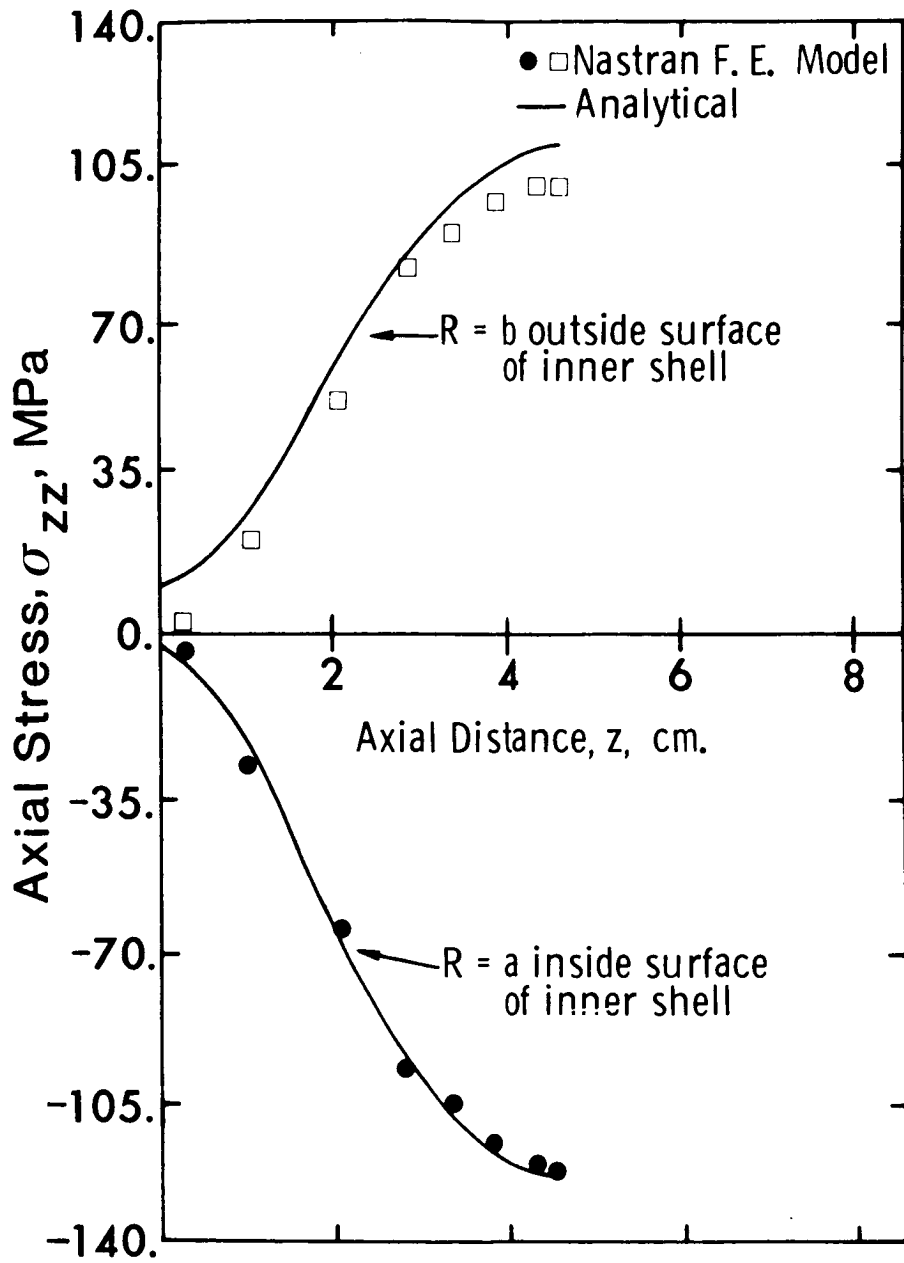


Fig. 5 Variation of axial stresses.

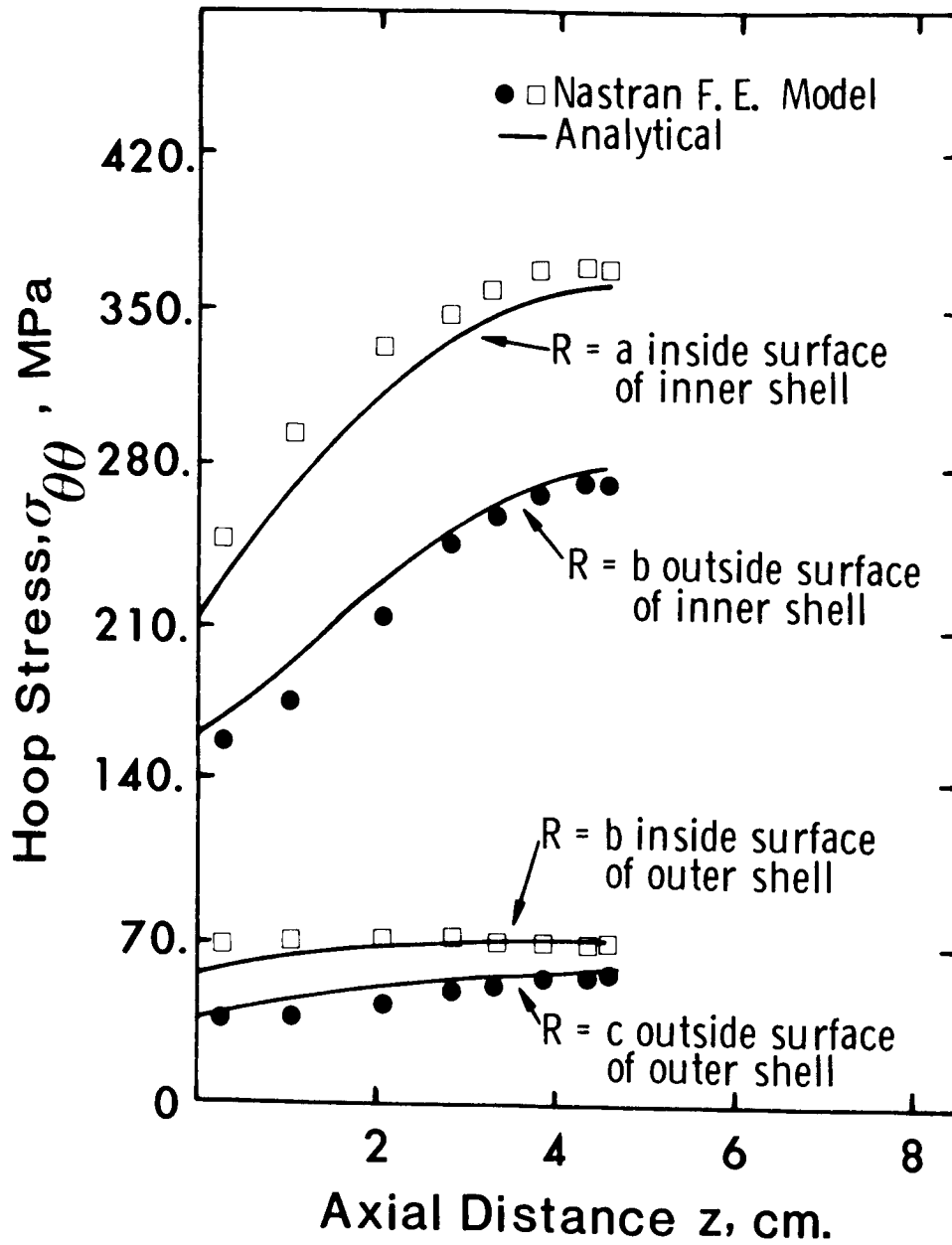


Fig. 6 Variation of hoop stresses with axial distance.

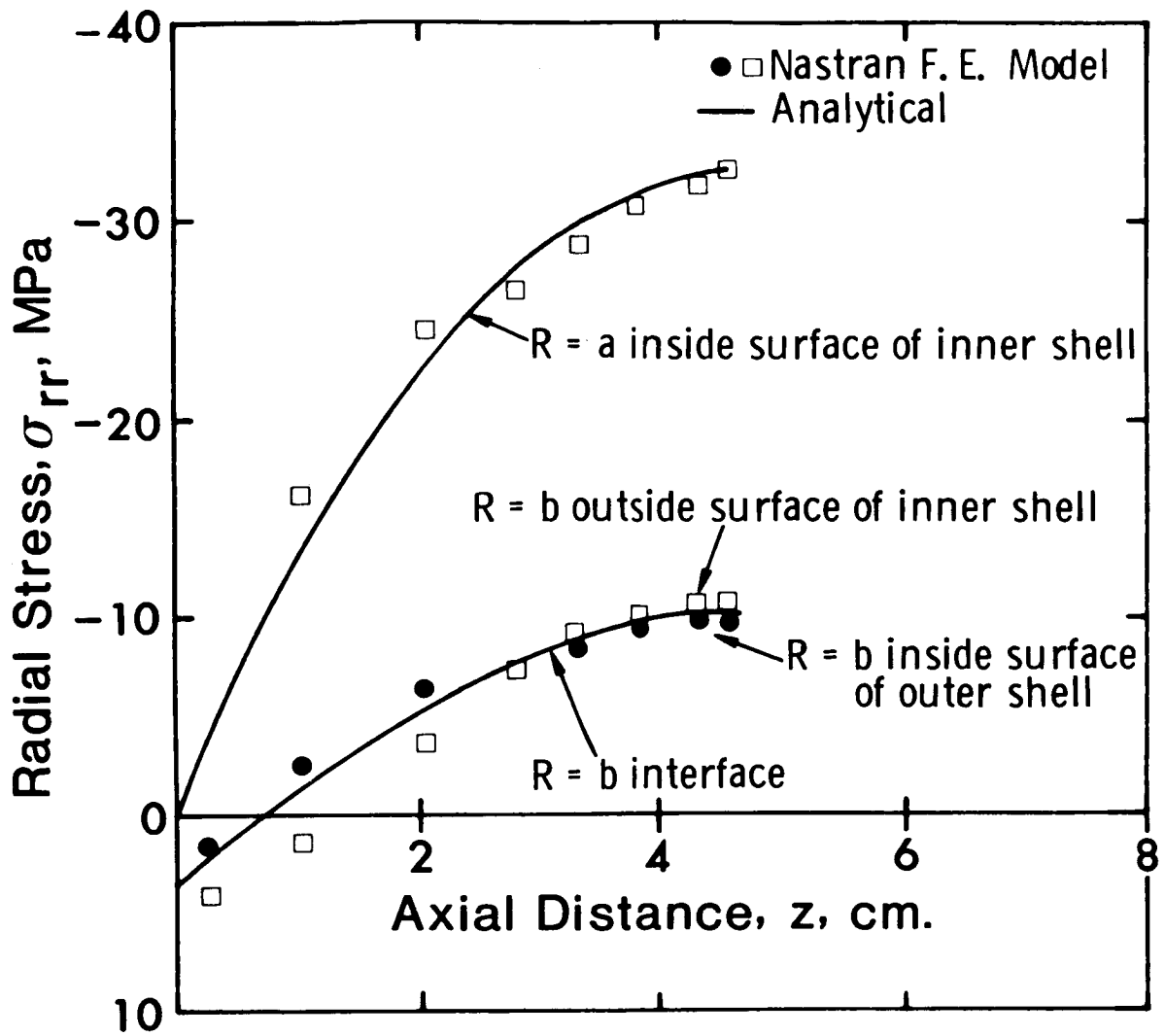


Fig. 7 Variation of radial stresses with axial distance.

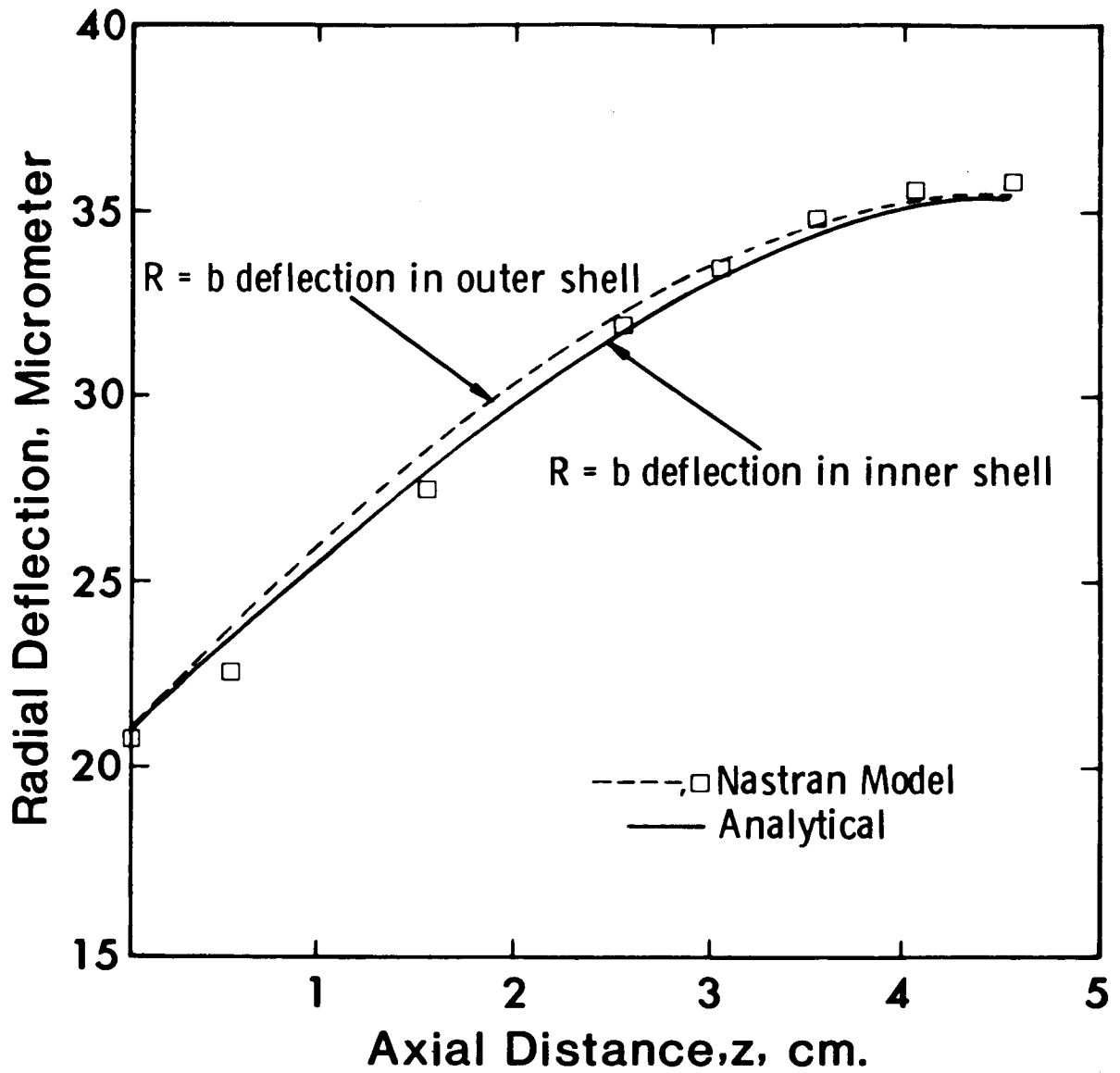


Fig. 8 Variation of radial deflections with axial distance z .

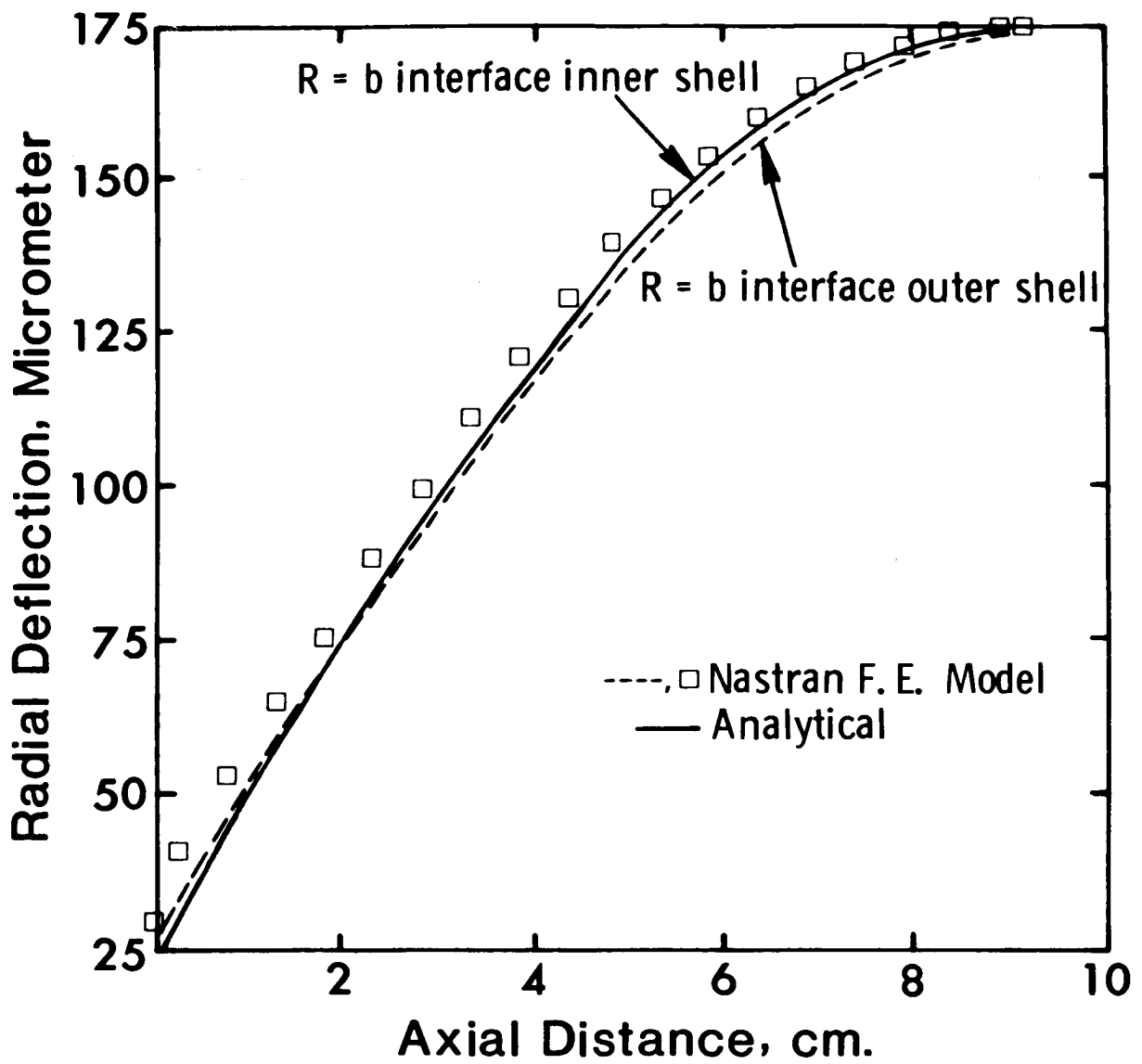


Fig. 9 Variation of radial deflection.